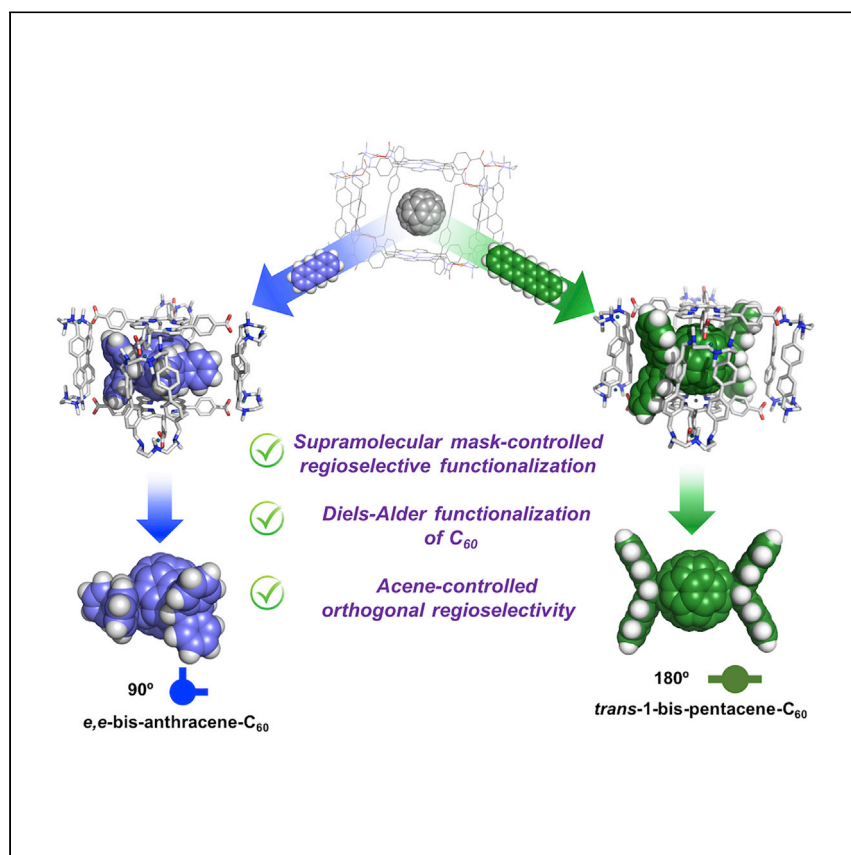Article

Regioselective access to orthogonal Diels-Alder C_{60} bis-adducts and tris-heteroadducts via supramolecular mask strategy

Supramolecular mask-controlled regioselective functionalization ✓

Diels-Alder functionalization of C_{60} ✓

Acene-controlled orthogonal regioselectivity ✓

90° → e,e-bis-anthracene-C_{60}

180° → trans-1-bis-pentacene-C_{60}

Supramolecular masks can be used to prepare C_{60} regioselectively. Pujals et al. use tetragonal prismatic nanocapsules to control the Diels-Alder reaction of encapsulated C_{60} with acenes, achieving orthogonal switching from 90° (e,e-bis-anthracene-C_{60}) to 180° (trans-1-bis-pentacene-C_{60}) functionalization by enlarging the acene and providing access to equatorial tris-heteroadducts via Bingel cyclopropanation of encapsulated mono- or bis-Diels-Alder adducts.

Míriam Pujals, Tània Pèlachs, Carles Fuertes-Espinosa, Teodor Parella, Marc Garcia-Borràs, Xavi Ribas

marc.garcia@udg.edu (M.G.-B.)
xavi.ribas@udg.edu (X.R.)

Highlights

Orthogonal synthesis of Diels Alder bis-C_{60} adducts via supramolecular masks

Acene-length-dependent isolation of e,e-bis-anthracene-C_{60} and trans-1-bis-pentacene-C_{60}

Equatorial hetero-tris-functionalized-C_{60} adducts combining Diels-Alder with Bingel reactions

Computational modeling as key tool to rationalize the role of supramolecular masks

Article

Regioselective access to orthogonal Diels-Alder C$_{60}$ bis-adducts and tris-heteroadducts via supramolecular mask strategy

Míriam Pujals,[1] Tània Pèlachs,[1] Carles Fuertes-Espinosa,[1] Teodor Parella,[2] Marc Garcia-Borràs,[1,3,*] and Xavi Ribas[1,4,5,*]

SUMMARY

The regioselective polyfunctionalization of highly symmetric spherical I_h-C$_{60}$ is extremely challenging and usually leads to the formation of regioisomeric mixtures not amenable for high-pressure liquid chromatography (HPLC) purification. Here, we pioneer the use of tetragonal prismatic nanocapsules to perform selective Diels-Alder (DA) functionalization of encapsulated I_h-C$_{60}$ using acenes. The supramolecular mask allows the regioselective synthesis of either e,e-bis-anthracene-C$_{60}$ (functionalization at 90°) or the synthesis of $trans$-1-bis-pentacene-C$_{60}$ (functionalization at 180°) by changing only the acene length. Moreover, the mask strategy allows one to obtain unprecedented equatorial hetero-tris-functionalized-C$_{60}$ adducts combining Diels-Alder with Bingel mask regiofunctionalization. Computational modeling provides crucial insights to rationalize the regioselective control exerted by the supramolecular mask on the successive DA cycloadditions. Molecular dynamics (MD) simulations revealed significant differences in the host-guest interactions and equilibrium established between the first-formed anthracene- and pentacene-based mono-adducts with the nanocapsule, which finally determine the observed orthogonal regioselectivity.

INTRODUCTION

The controlled regioselective polyfunctionalization of icosahedral isomer I_h-C$_{60}$ is a very challenging task that was clearly identified soon after the discovery of fullerenes.[1–4] Because of its high symmetry, usually the functionalization of fullerenes with multiple addends leads to mixtures of non-equivalent regioisomers, and their purification using multistep high-pressure liquid chromatography (HPLC) separation is tedious and usually not practicable.[5,6] Pioneers in the field designed non-chromatographic synthetic strategies in the 1990s to overcome the intractable complex mixtures of regioisomers commonly obtained, with the tether-directed remote functionalization reported by Diederich[7,8] and the "orthogonal transposition" synthetic method developed by Kräutler[9,10] being the mainstream strategies. However, these protocols bear important drawbacks, since (1) tethers cannot be removed and are left on the fullerene derivative, unless cleavable di-$tert$-butylsilylene protecting groups within the tether are used,[11,12] and (2) high temperatures are required (>180°C) to synthetize pure polyderivatives at the solid state, such as the synthesis of $trans$-1-bis-anthracene-C$_{60}$, which was further used as a template to obtain equatorial tetrakis-C$_{60}$ adducts by means of Bingel cyclopropanation.[9] In short, the synthesis of regioisomerically pure polyderivatives, if attainable, is envisioned as a
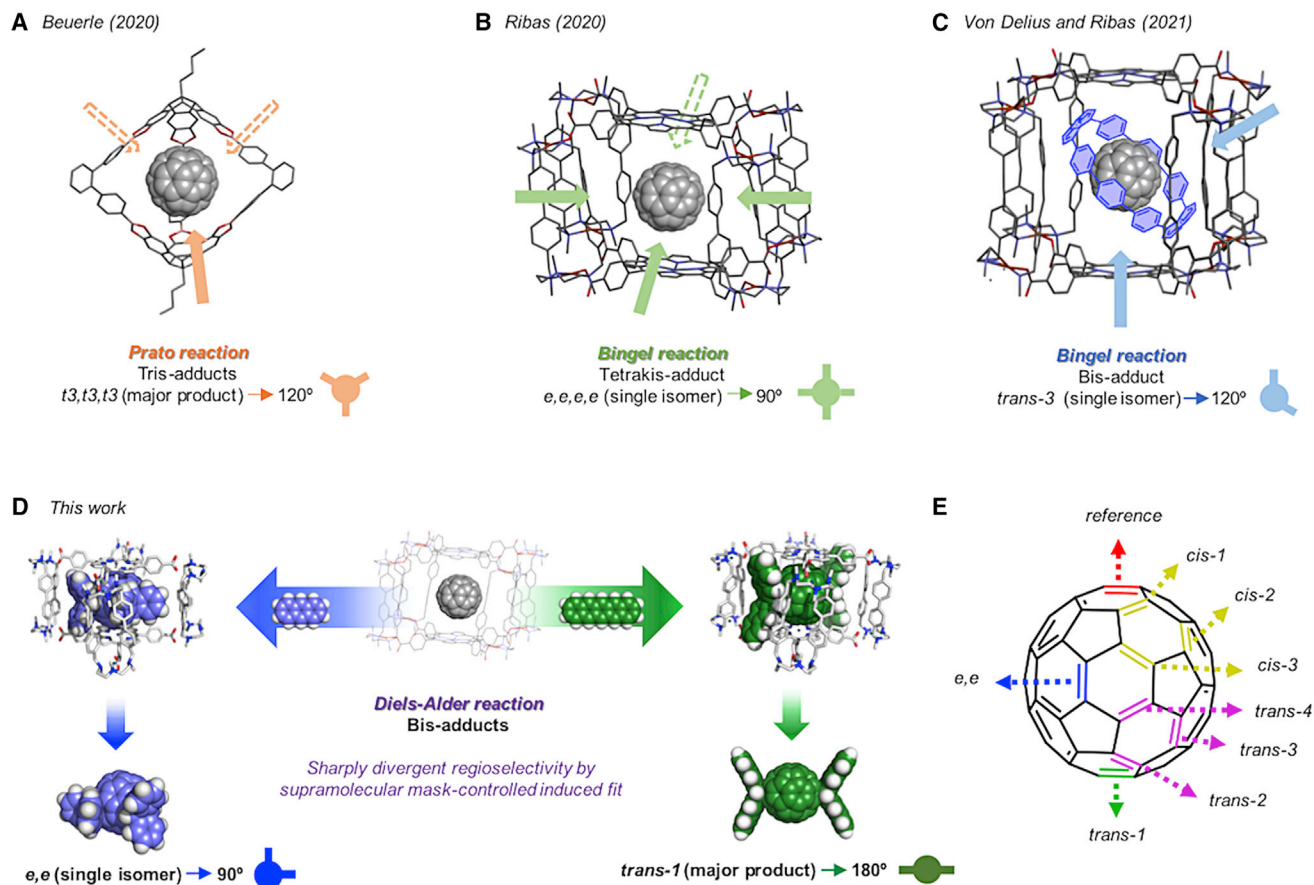
Figure 1. Strategies reported for the regioselective synthesis of C_{60} polyadducts

(A) Host-guest complex featuring a trigonal bipyramidal covalent organic cage to improve the regioselectivity of the Prato reaction on C_{60}. The *t3,t3,t3*-tris-adduct is obtained as the major product in a mixture of four regioisomers.

(B) Host-guest complex featuring a tetragonal prismatic nanocapsule to regiofunctionalize C_{60} through the four cross-shaped gates of the cage. The *e,e,e*-tetrakis-adduct is obtained as the unique regioisomer.

(C) Matryoshka-like three-shell complex featuring a prismatic tetragonal cage that encapsulates an aromatic [10]cycloparaphenylene ring and, in turn, C_{60} fullerene. The symmetry-mismatched *trans*-3-bis-adduct is obtained as the unique product of the reaction.

(D) This work: extension of the supramolecular mask strategy to Diels-Alder reactivity to obtain chemo- and regioselectively the *e,e*-bis-An-C_{60} or the *trans*-1-bis-Pn-C_{60} depending solely on the different host-guest equilibria established due to the acene.

(E) Diagram of the second addition to a C_{2v}-symmetrical C_{60} mono-adduct (first addend is the reference).

brake-lift opportunity for their broad applicability, allowing the incorporation of these compounds into many types of materials and devices.[6]

Recently, we have pioneered the use of supramolecular tetragonal prismatic nanocapsules with a dual purpose: (1) first, to serve as high-affinity hosts of C_{60},[13] and (2) second, to be used as supramolecular masks for the regioselective functionalization of the trapped fullerene,[14,15] by exposing limited portions of its surface through the windows of the nanocapsule. Specifically, the supramolecular mask allowed the regioselective Bingel cyclopropanation of C_{60} through the cross-shaped windows of the nanocapsule, simultaneously withstanding the reaction conditions. In this manner, isomer-pure polyadducts featuring from two to four addends along the equatorial belt were synthesized, i.e., bis-, tris-, and tetrakis-adducts (Figure 1B).[14] More recently, a more sophisticated three-shell matryoshka-like complex was used to further restrict the exposed surface of the encapsulated C_{60}, obtaining exclusively the pure Bingel *trans*-3-bis-diethylmalonate-C_{60} adduct (Figure 1C).[16] It should be

noted that the highly symmetric *trans*-1 bis-adduct is electronically highly disfavored and stands as the Holy Grail for C_{60} bis-functionalization. In addition, Beuerle and coworkers reported in 2020 the use of a trigonal bipyramidal covalent organic cage as a shadow mask for the regioselective 1,3-dipolar Prato functionalization of trapped C_{60} (Figure 1A),[17] obtaining predominantly symmetry-matched tris-adducts as a mixture of four regioisomers (of 46 possible). Therefore, a nanocapsule fullerene host of a given symmetry and a specific number of windows can *a priori* meet the requirements, but most importantly, the mask has to survive the necessary reaction conditions.

Herein, we report the extension of the supramolecular mask strategy to the Diels-Alder (DA) functionalization of C_{60} using different acenes (anthracene [An] versus pentacene [Pn]; Figure 1D), featuring a sharply divergent and controlled regioselectivity by changing only the length of the acene: by using An, an equatorial bis-adduct is obtained, while a *trans*-1-bis-adduct is achieved when Pn is used as the acene of the reaction (Figure 1E). Moreover, the mask strategy allows the obtention of equatorial hetero-tris-functionalized-C_{60} adducts combining DA with Bingel mask regiofunctionalization. Computational modeling combining molecular dynamics (MD) simulations and electronic structure analyses afford a clear understanding of the regioselective control achieved by the nanocapsule. Simulations demonstrated that a different host-guest equilibrium occurs between the nanocapsule and the An and Pn mono-adducts. The different accommodations of the respective mono-adducts in the supramolecular mask differently limit which positions are accessible for a selective DA bis-functionalization, thus leading to a different bis-functionalization pattern.

RESULTS AND DISCUSSION

Regioselective Diels-Alder bis-functionalization of C_{60} using the supramolecular mask strategy

We started the present study challenging the use of the tetragonal prismatic nanocapsules $\mathbf{1a} \cdot (BArF)_8$ (Pd^{II}-based)[13] and the analogs $\mathbf{1b} \cdot (BArF)_8$ (Cu^{II}-based)[18,19] as masks for the regioselective DA functionalization. Previous analysis indicated an excellent affinity between $\mathbf{1a} \cdot (BArF)_8$ and C_{60} fullerene (association constant K_a = 2.8 (± 0.6) $\times$ 10^7 M^{-1}).[13] These hosts also showed a remarkable breathing effect, since the Zn-Zn interdistance between porphyrin subunits of the nanocapsule swings from 14.1 Å when the cavity is empty to 13.1 Å upon C_{60} encapsulation, as observed from X-ray structures and computational modeling. Moreover, a combined NMR and computational modeling study provided a detailed description of the binding process and stability of fullerenes in the cavity of this nanocapsule $[\mathbf{1a}]^{8+}$.[20] That study highlighted the specific role of the porphyrin phenyl rings (Figure 1B), which explore different conformations for permitting the smooth entrance of fullerenes without disassembly of the cage and for maintaining them in the center of the cavity. Regarding the stability of the host-guest complexes under the reaction conditions, the mild DA reaction conditions compared with the previously reported successful Bingel functionalization[14] were envisioned as convenient for the overall stability of the nanocapsule along the reaction course.

As expected, the reaction of $C_{60} \subset \mathbf{1a} \cdot (BArF)_8$ with 30 equiv of An in CH_3CN at 50°C for 48 h afforded bis-adducts as the main product, with the minor presence of mono-adduct in a ratio of 1:0.4, as monitored by high-resolution mass spectrometry (or HRMS) (Figures 2C and S1). Although HRMS is not a quantitative technique, previous work has demonstrated that it is a useful semi-quantitative technique to monitor these fullerene functionalization reactions by using nanocages.[13,14,16] Attempts to increase the ratio toward bis-adducts have been unsuccessful due to the interplay
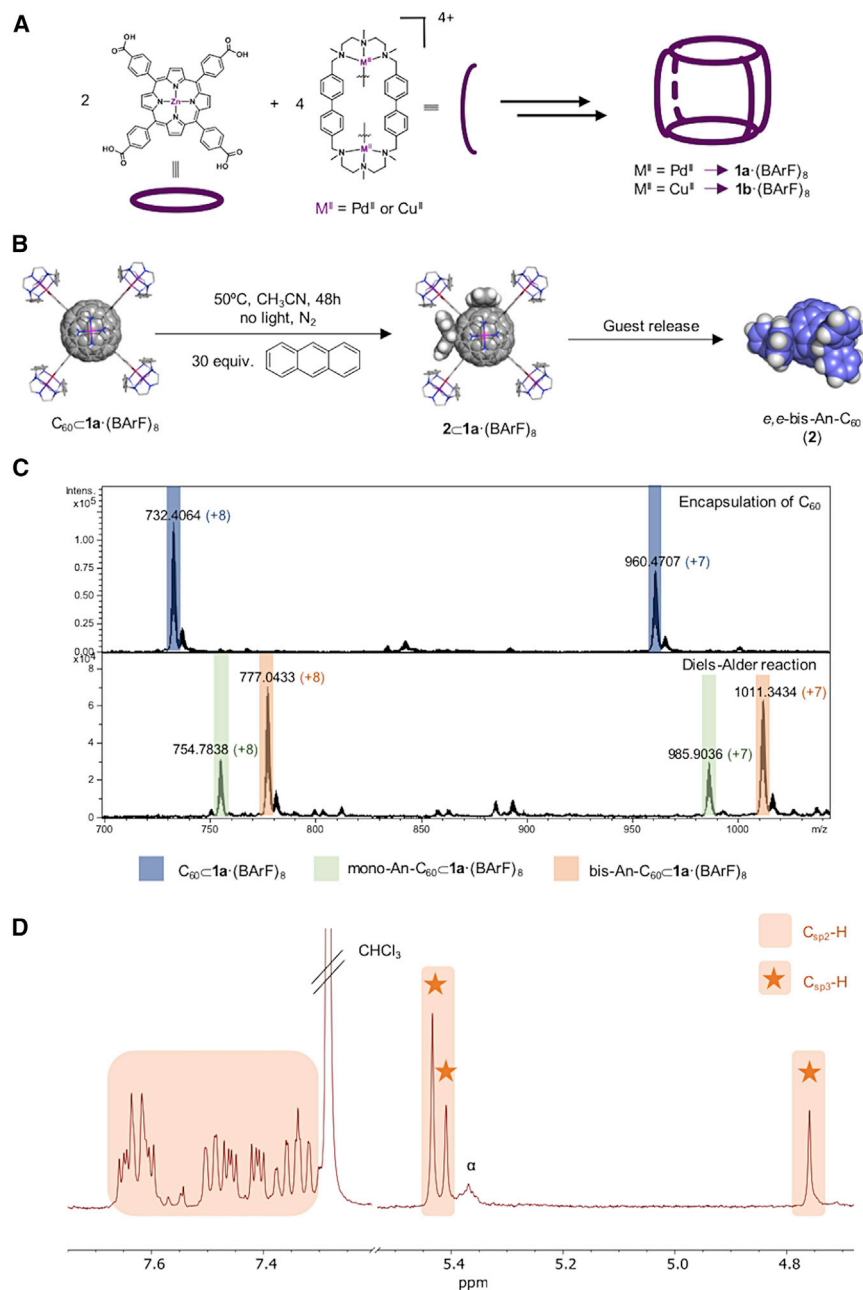
Figure 2. Synthesis and characterization of *e,e*-bis-An-C$_{60}$ (2)

(A) Schematic synthetic protocol of tetragonal prismatic nanocapsules **1a**·(BArF)$_8$ and **1b**·(BArF)$_8$.

(B) Chemo- and regioselective synthesis for **2** using **1a**·(BArF)$_8$ as a supramolecular mask.

(C) HRMS monitoring of the synthesis of **2**⊂**1a**·(BArF)$_8$.

(D) ^{1}H NMR of **2**. In orange, signals corresponding to protons of anthracene addends (highlighting with a star the cycloadded C$_{sp3}$ protons). α, peak corresponding to preparative TLC silica. See also Figures S1–S11.

of the retro-DA reaction (Figure S3A). The functionalized product was easily released from the cage by using an easy solvent-washing protocol[13] with CHCl$_3$ and, remarkably, a single bis-An-C$_{60}$ isomer was found, which was isolated in 38% yield (HPLC crude also shows the presence of tris-adducts in minor amounts, which are formed during the workup, see Figure S3B). NMR characterization clearly indicated that

the equatorial regioisomer (*e,e*-bis-An-C_{60}, **2**) was solely formed among bis-adducts, with a distinctive 2:1:1 signal pattern between 4.6 and 5.6 ppm (rising from the C_s symmetry of the product). This characteristic distribution of signals corresponds to the cycloadded C_{sp3}-H protons of the two An addends of the bis-adduct in an equatorial fashion (Figures 2D, S5–S11, and S68). This represents a very remarkable control of the regioselectivity, as previous DA functionalization studies showed that bare C_{60} affords complicated mixtures of bis- and tris-An adducts, and among the bis-adducts, a mixture of five different isomers was found (16% *ee*, 1.3% *trans*-1, 13% *trans*-2, 26% *trans*-3, 10% *trans*-4).[21,22]

To gain insight into the host-guest equilibrium established by the encapsulated mono- and *e,e*-bis-An-C_{60} adducts and the nanocapsule, MD simulations were performed (see computational details in the supplemental experimental procedures). For each system, three replicas of MD trajectories of 1,000 ns each (accumulating a total of 3 μs of simulation time) were carried out using the modeled **1a**·(Cl)$_8$ considering an explicit solvent box of acetonitrile.[14] Regarding the mono-An-C_{60} system, MD simulations revealed that gate-to-gate rotation of the An addend can effectively occur (Figures 4A and S69A–S71A and Video S1). MD simulations describe that these gate-to-gate rotations take place at the nanosecond-to-microsecond timescale, as different rotations are observed throughout the 1,000 ns of simulation time. Therefore, it is expected that the An moiety can explore the four symmetric gates of the capsule indistinctively, albeit longer MD trajectories would be required for the An moiety to equally visit all the nanocapsule gates during the simulations.

The relative orientation of the An moiety with respect to the porphyrin units of the capsule was also analyzed. The An addend can be oriented parallel to the porphyrin moieties or perpendicular to them (Figure 4B and S69B–S71B). MD simulations indicated that the interconversion between the two orientations occurs fast, being that the mono-adduct spins along its C_{2v} axis, and that both orientations are indistinctively explored by the An addend. Therefore, a highly dynamic host-guest equilibrium of the encapsulated mono-adduct is described by simulations, including both the gate-to-gate rotation of the adduct and the spinning around the mono-An-C_{60} C_{2v} axis. In contrast, MD simulations for the encapsulated *e,e*-bis-An-C_{60} (**2**) revealed that the gate-to-gate rotation of the An groups within the nanocapsule is completely restricted and each An moiety is fixed to a single gate (Figures S72A–S74A and Video S2). In addition, no spinning of the bis-adduct is observed (Figures S72B–S74B). This indicates that the second An is responsible for restricting the rotation and dynamics of the fullerene adduct in the nanocapsule.

To understand the high regioselectivity achieved for the bis-adduct formation, the frontier molecular orbitals (FMOs) involved in the DA reaction for the mono-An-C_{60} adduct were also analyzed.[23,24] The highest occupied molecular orbital (HOMO) of the diene (i.e., An) and the low-lying lowest unoccupied molecular orbitals (LUMOs) of the dienophile (i.e., mono-adduct) were studied while considering the geometric restrictions of the An mono-adduct in the host-guest complex (Figure 5, S82, and S83). The mono-An-C_{60} LUMO (−0.090 eV) has the appropriate antibonding orbital contributions on the *equatorial* bond (*e* bond; Figures 5[1a], 5[1b], S82A, and S82B), while close in energy, LUMO+1 (0.117 eV) has orbital antibonding lobes localized on the *equatorial-prime* bond (*e′* bond, Figures 5[2a], 5[2b], S82A, and S82B). Functionalization of any of these two bonds (*e* and *e′*) of the mono-adduct would lead to the same bis-adduct product by symmetry (*e-e* and *e-e′* bis-adducts are equivalent). Because of the dynamic host-guest equilibrium and the spin rotation of the mono-An-C_{60} characterized by MD simulations, both equatorial bonds (*e* and

e') can be exposed to the nanocapsule open gate (Figures 5[1a] and 5[2b]), depending on the orientation of the An addend. Other bonds on the mono-An-C_{60} surface also exhibit appropriate antibonding LUMO or LUMO+1 contributions; however, their functionalization is restricted due to sterics imposed by the nanocapsule. On the other hand, the *trans*-1 bond has reactive antibonding orbital contributions only in the LUMO+2, and it is accessible from the opposite gate of the nanocapsule (Figures 5[3a], 5[3b], and S82A). However, the significantly higher energy of this LUMO+2 molecular orbital (0.411 eV) with respect to the LUMO and LUMO+1 makes the *trans*-1 bond kinetically much less reactive than the equatorial ones. Taking together the steric control imposed by the nanocapsule, the dynamic equilibrium exhibited by the host-guest complex, and the distribution of reactive mono-An-C_{60} FMOs, the kinetically most favorable second DA addition is expected to be at one of the equatorial positions rather than at *trans*-1, leading to the exclusive formation of the observed equatorial *e,e*-bis-An-C_{60} (**2**), which also corresponds to the thermodynamically more stable product (Figure S88 and Table S1).

Regioselective orthogonal Diels-Alder bis-functionalization of C_{60} combining the supramolecular mask strategy and acene length for steric control

At this stage, we reasoned that extending the acene molecule could infer a larger steric restriction that would fix the mono-adduct addend position along the vertical of a nanocapsule's rectangular window (perpendicular to the porphyrins), and that it might affect the nature of the bis-adduct formed. Gratifyingly, the reaction of $C_{60} \subset \mathbf{1a} \cdot (BArF)_8$ with 2.1 equiv of Pn in CH_3CN/CH_2Cl_2 (4/1) at 65°C for 16 h afforded bis-adduct as the main product (only traces of mono-adduct were present), as assessed by HRMS (Figure 3B) and HPLC (Figure S16). Strikingly, upon nanocapsule disassembly and workup, bis-adducts were obtained in 79% yield (HPLC in Figure S16), since a few quantities of tris-adducts were formed during the workup. As can be seen in the crude HPLC chromatogram (Figure S16), there is a predominant peak (retention time 7.576 min, dotted box of the HPLC chromatogram), which represents 78% of the bis-adducts. Nevertheless, it was purified through a simple preparative thin-layer chromatography (TLC) and was isolated in 30% yield due to insolubility issues of this product. NMR characterization confirmed that this predominant bis-adduct was the unprecedented D_{2h} *trans*-1-bis-Pn-C_{60} (**4**), with a unique distinctive singlet at 6.32 ppm corresponding to the cycloadded C_{sp3} protons of the Pn addends in a *trans*-1 fashion (Figures 3C, S18–S19, and S68). A high-field shifting of methine protons of **2** can be observed in comparison with methine protons of **4**, due to the anisotropic effect induced by the ring currents of adjacent aromatic rings. In the case of **2**, the An addends are placed perpendicularly and facing each other and the anisotropic effect of the aromatic protons from one addend produces a considerable shielding effect of the methine protons from the other addend (5.43, 5.41, and 4.76 ppm, Figure 2D). In the case of **4**, since Pn addends are placed at 180° to the fullerene sphere, this effect is not noticed by methine protons and their shifts are higher (6.32 ppm, Figure 3C). The minor peaks at 6.22, 8.44, and 8.62 correspond to the isomerization of both Pn moieties to formed non-symmetric addends (see Figure S18B), but the regioselectivity of the product remains intact as *trans*-1 (i.e., addends at 180°). Compared with the reactivity of bare C_{60} with Pn, a mono-adduct is obtained in 59% yield alongside seven bis-Pn adducts in a combined 13% yield and not distinguishable by ^{1}H NMR.[25] Also, a mixture of mono-adduct and mixtures of regioisomers were obtained when the reaction was performed in the solid state through ball-milling.[26]

The striking differences in regiofunctionalization between An and Pn deserved further insight. First, MD simulations were carried out with encapsulated mono-Pn-C_{60} (**3**), to study the new host-guest complex. Simulations revealed that gate-to-gate rotation of
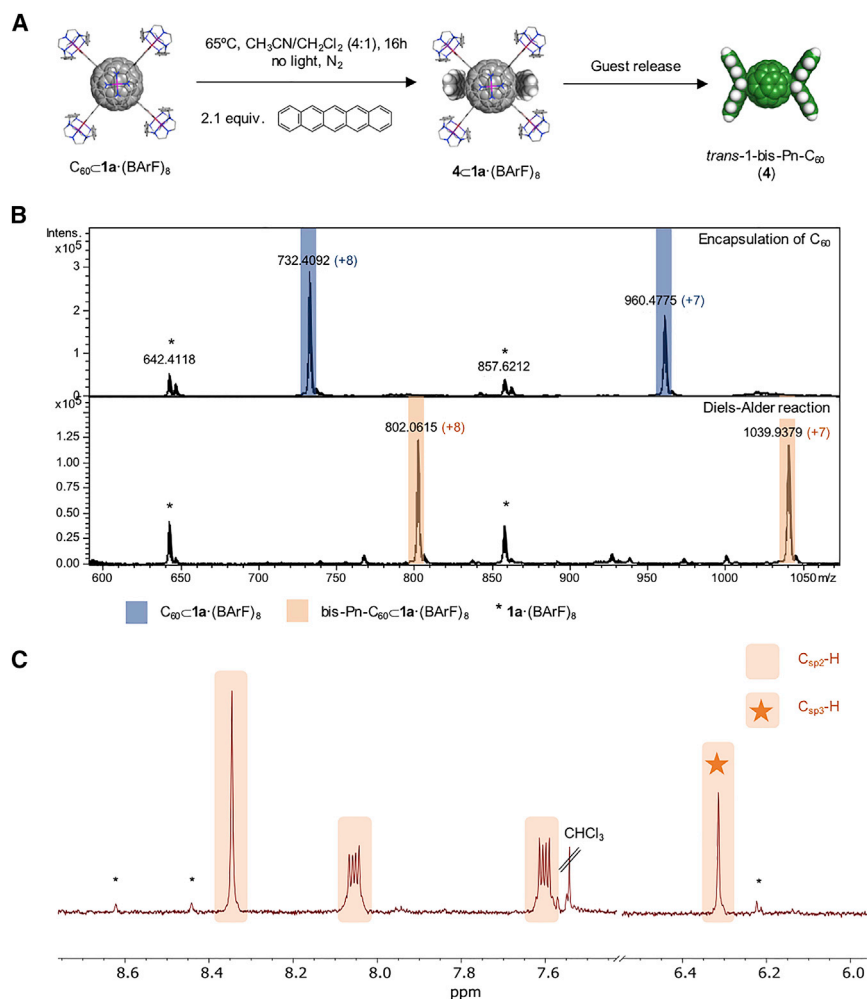
Figure 3. Synthesis and characterization of *trans*-1-bis-Pn-C$_{60}$ (4)
(A) Schematic representation of the synthesis of **4**.
(B) HRMS monitoring of the synthesis of **4**⊂**1a**·(BArF)$_8$.
(C) ^{1}H NMR of **4**. In orange, signals corresponding to protons of pentacene addends (highlighting with a star the cycloadded C$_{sp3}$ protons). *Signals corresponding to the minor isomer (due to isomerization of pentacene addends). See also Figures S15–S19.

the Pn moiety is completely restricted, and no gate-to-gate transitions are observed along the microsecond timescale MD trajectories (Figures 4C and S75A–S77A and Video S3). In this case, the Pn moiety remains in a single gate of the capsule throughout the simulation time, in sharp contrast to what was observed for mono-An-C$_{60}$, where gate-to-gate rotation events are observed at this timescale. In addition, analyses of MD trajectories showed that the mono-Pn-C$_{60}$ adduct explores a single orientation, vertical with respect to the nanocapsule (Figures 4D and S75B–S77B). Within this orientation, the Pn moiety is placed perpendicular to the porphyrin units due to the steric hindrance that the molecular clips of the nanocapsule exert to the extended acene. Therefore, the bulkier Pn addend completely fixes the mono-Pn-C$_{60}$ adduct (**3**) in a single orientation, opposite to the dynamic equilibrium observed for the mono-An-C$_{60}$ host-guest system. MD simulations with the encapsulated *trans*-1-bis-Pn-C$_{60}$ (**4**) also showed that the guest is, as expected, fixed in a unique orientation, with the Pn addends perpendicular to the porphyrins (Figures S78–S80).
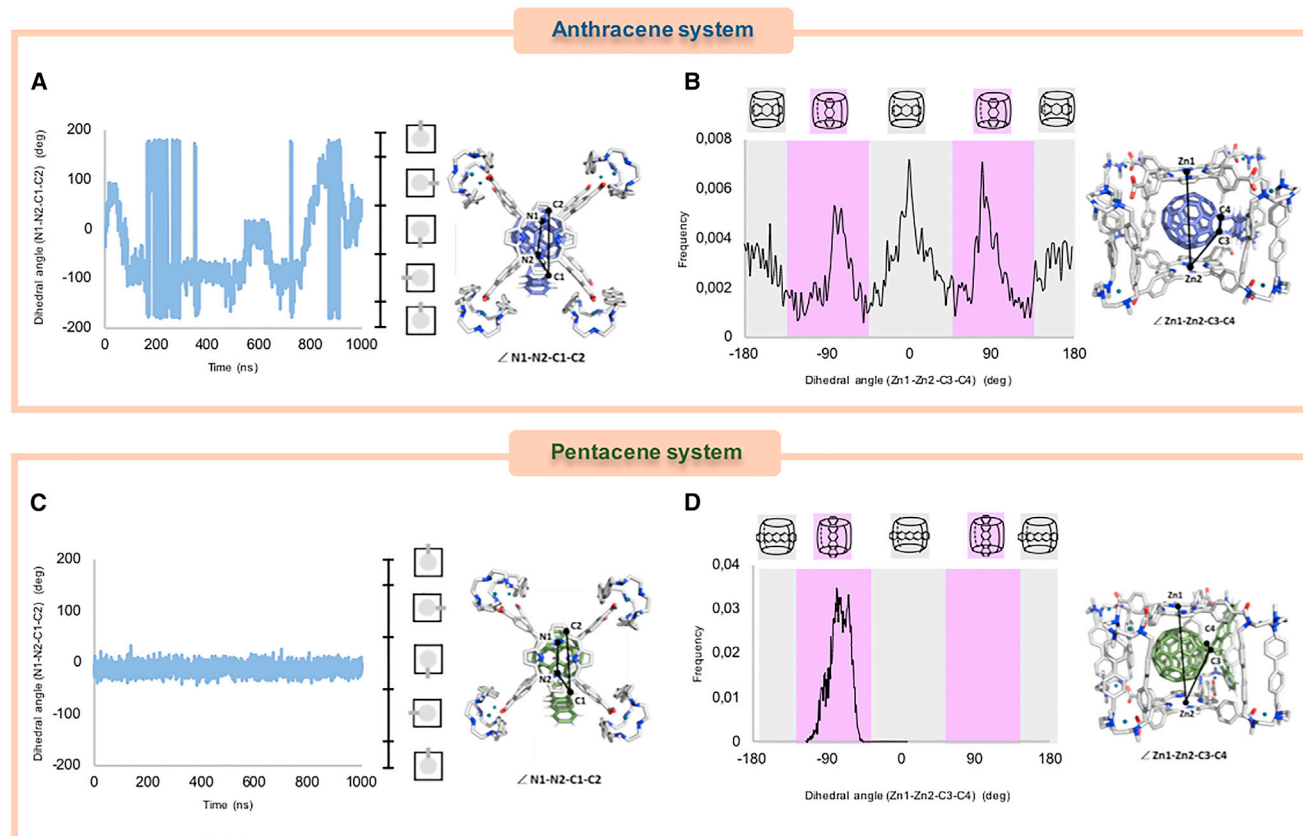
Figure 4. Analysis and characterization of the host-guest equilibria of mono-An-C$_{60}$⊂1a·(Cl)$_8$ and mono-Pn-C$_{60}$⊂1a·(Cl)$_8$ using MD simulations

Analysis of anthracene mono-adduct dynamics inside the nanocage.

(A) ∠N1-N2-C1-C2 dihedral angle describes the relative rotation of the encapsulated mono-An-C$_{60}$ with respect to the nanocapsule gates along the MD simulation time. N1 and N2 are atoms from the porphyrin, while C1 and C2 are atoms from the fullerene derivative (see scheme). Different values explored for the ∠N1-N2-C1-C2 dihedral angle along the simulation time describe gate-to-gate rotations of the fullerene addend (see Figures S69–S71 for additional replicas).

(B) ∠Zn1-Zn2-C3-C4 dihedral angle describes the relative orientation of the fullerene acene addend with respect to the nanocapsule porphyrins. Zn1 and Zn2 are atoms from the porphyrins, while C3 and C4 are atoms from the fullerene derivative (see scheme). The presented histogram plot (180 bins of 2° each) describes the most visited ∠Zn1-Zn2-C3-C4 dihedral values during the 1,000 ns MD trajectory. Different values explored by the ∠Zn1-Zn2-C3-C4 dihedral angle along the MD trajectory show that the anthracene addend can be equally oriented parallel or perpendicular to the nanocapsule porphyrins, being that the mono-An-C$_{60}$ spins along its C$_{2v}$ axis (see Figures S69–S71 for additional replicas).

(C and D) Equivalent analyses for pentacene mono-adduct dynamics inside the nanocage (mono-Pn-C$_{60}$⊂1a·(Cl)$_8$ system), respectively. See also Figures S75–S77 for additional replicas.

To rationalize the impact that the restricted dynamism of the encapsulated mono-Pn-C$_{60}$ (3) has on the second DA functionalization, reactive FMOs were also analyzed considering the geometrical restrictions imposed by the encapsulation similar to the An case (see discussions above).

Within the single orientation that mono-Pn-C$_{60}$ explores when formed inside the nanocapsule, with the Pn unit vertically aligned (pointing perpendicular to the porphyrins), the first LUMO orbital (−0.095 eV) does not have antibonding contributions localized on any bond that is easily accessible from the nanocapsule open gates (Figures 5[1c] and S85–S86). Low-lying LUMO+1 (0.114 eV) has appropriate antibonding lobes on the *e*′ bond that could lead to an effective DA reaction with the Pn HOMO (Figures 5 [2c] and S85). Nevertheless, the *e*′ bond of the encapsulated mono-Pn is oriented perpendicular to the porphyrins, which implies that the second Pn unit should approach parallel to the porphyrins (horizontally aligned) for reaction. However, due
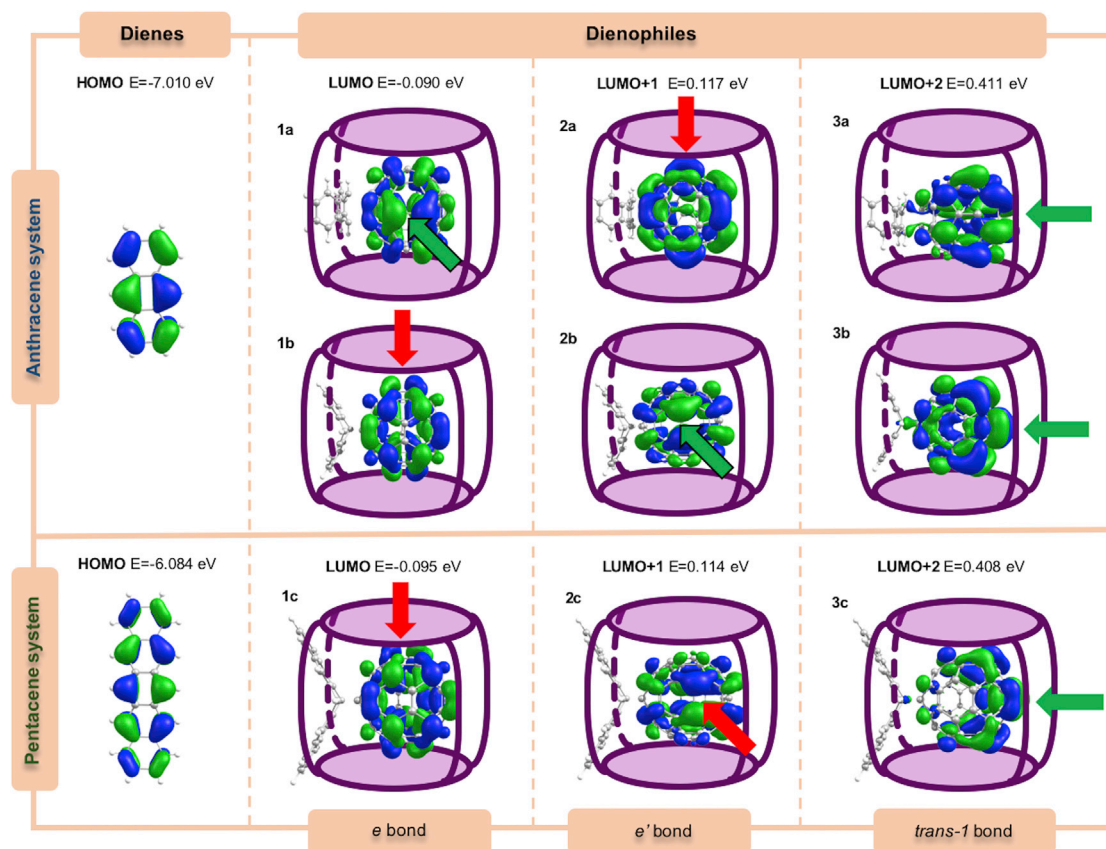
Figure 5. Frontier molecular orbitals (FMO) involved in the Diels-Alder cycloadditions

HOMOs of the acenes (anthracene and pentacene) and low-lying LUMOs of the corresponding mono-adducts are reported (HF/6-31G(d,p), energies given in eV, see the supplemental experimental procedures for computational details). A schematic representation of the mono-adducts' LUMOs when encapsulated is shown. For the anthracene system, two possible orientations of the mono-adduct are depicted inside the nanocapsule, considering its possible rotation as characterized from MD simulations (Figure 4B): anthracene addend oriented in parallel (1a, 2a, and 3a) or perpendicularly (1b, 2b, and 3b) with respect to the porphyrins. For the pentacene system, only one orientation of the mono-adduct is depicted inside the nanocapsule, since its rotation is limited due to steric hindrance as observed from MD simulations (Figures 4D and S75–S77): pentacene moiety oriented perpendicularly with respect to the porphyrins (1c, 2c, and 3c). See also Figures S82–S88 and Table S1 for further information and discussion.

to the larger size of the Pn and its clashing with the molecular clips, this reactive approach for functionalizing the e' bond in encapsulated mono-Pn-C$_{60}$ would be highly disfavored. Hence, mono-Pn-C$_{60}$ should preferentially react through the less reactive LUMO+2 orbital (0.408 eV) that has appropriate antibonding lobes localized on the *trans*-1 bond (Figures 5[3c], S81A, and S85), which is oriented parallel to the porphyrins. This relative orientation of the *trans*-1-bond makes it suitable for effectively reacting with the bulkier Pn, which can easily approach this reactive bond in a vertical alignment, parallel to the porphyrins, without any steric hindrance. Therefore, although the LUMO+2 orbital with appropriate antibonding contributions on the *trans*-1-bond for DA reaction is expected to be kinetically less reactive than LUMO or LUMO+1, geometric restrictions imposed by the supramolecular mask favor the regioselective formation of the *trans*-1-bis-Pn-C$_{60}$⊂**1a**·(Cl)$_8$ product through the participation of LUMO+2, which also corresponds to the thermodynamically less stable product in the absence of the nanocapsule (Figure S88 and Table S1). Thus, the orthogonal regiofunctionalization of C$_{60}$ to form either the *trans*-1-bis-adduct with Pn or the equatorial *e,e*-bis-adduct with An is driven solely by the different host-guest equilibrium reached by
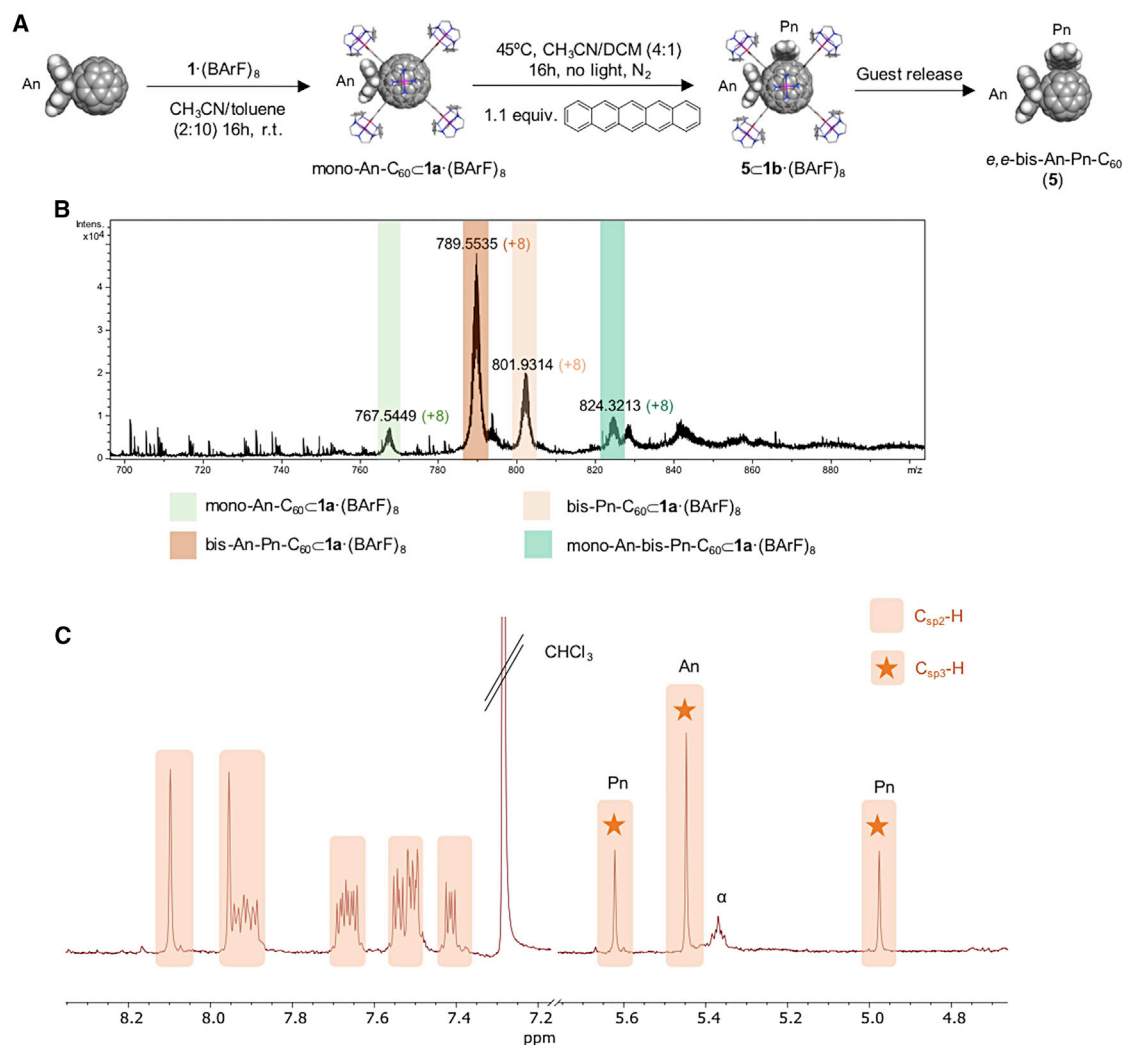
Figure 6. Synthesis and characterization of *e,e*-bis-An-Pn-C$_{60}$ (5)
(A) Schematic representation of the synthesis of **5**.
(B) HRMS of the crude reaction of the synthesis of **5** ⊂ **1a**·(BArF)$_8$.
(C) ^{1}H NMR of **5**. In orange, signals corresponding to protons of pentacene addends (highlighting with a star the cycloadded C$_{sp3}$ protons). α, peak corresponding to preparative TLC silica. See also Figures S20–S28.

the mono-adducts that depends on the accommodation of the acene addend within the supramolecular mask.

Finally, to differentiate second addition at the *e* bond or the *e'* bond, the synthesis of a hetero-DA-bis-adduct combining An and Pn was attempted (Figures 6, S20–S28, and S68). Mono-An-C$_{60}$, synthesized following reported procedures,[22,25] was fully encapsulated within **1a**·(BArF)$_8$, and 1.1 equiv of Pn was added. After 16 h at 45°C, the major product was the derivative bearing one An and one Pn addend, *e,e*-bis-An-Pn-C$_{60}$ (**5**), as can be seen by HRMS (Figure 6B). The bis-adduct formed was isolated and was characterized by 1D and 2D NMR. In the ^{1}H NMR, the 1:2:1 signal pattern in the region of 4.9–5.7 ppm can be clearly seen, which corresponds to the C$_{sp3}$-H protons of the acene addends (Figure 6C). As mentioned before, this unique pattern indicates the formation of an equatorial *e,e*-bis-adduct. By NOESY we determined that the singlet integrating two symmetrical protons at 5.45 ppm

corresponded to the An moiety (Figures S24 and S25); thus, the species is the *e,e*-bis-isomer, necessarily formed with the Pn moiety in vertical orientation within the mask. The latter confirmed the prediction based on MD studies indicating that solely the vertical orientation is possible for the Pn addend.

Controlled regioselective hetero-poly-functionalization of C_{60}

With the orthogonal *e,e*-bis-An-C_{60} (**2**) and *trans*-1-bis-Pn-C_{60} (**4**) as pure bis-adducts in hand, our new target was to submit them to Bingel cyclopropanation conditions under the supramolecular mask strategy, seeking the synthesis of pure-isomer hetero-poly-adducts. We rapidly noticed that reencapsulation of **2** in the Pd^{II}-based **1a**·$(BArF)_8$ was not efficient due to the rigidity of the gate entrances; thus, we resorted to the analogous more adaptable Cu^{II}-based nanocapsule **1b**·$(BArF)_8$,[18,19] which showed practically full encapsulation of the guest. We first focused our efforts in heterofunctionalizing the encapsulated *e,e*-bis-An-C_{60} (**2**) by reacting it with diethyl bromomalonate and NaH (Figure 7A).[14] HRMS monitoring showed that the expected equatorial hetero-tetrakis-adduct was formed, but in very small amount. In contrast, a tris-adduct, i.e., *e,e*-bis-An-*e*-mono-diethylmalonate-C_{60} (**6**), was the major product (Figures 7B, S29–S39, and S68). It was released from the nanocapsule by solvent washing with $CHCl_3$ and, after careful NMR and UV-vis spectroscopic analyses (Figures 7C and S31–S38), a mixture of two tris-regioisomers (isomers **6(I)** and **6(II)**) was characterized in a 1:3.7 ratio, respectively. For each isomer, the observed 1:1:1:1 distribution of signals corresponding to the aliphatic C_{sp3}-H of the An addends at a 1:1:1:1 ratio is the expected one. In the ^1H NMR of Figure 7C, from 4.8 to 5.6 ppm, can be clearly seen two sets of signals of four singlets each. In the region of 4.8–4.9 ppm, two singlets are observed with a 1:3.7 ratio (4.89 and 4.82 ppm, respectively), which are associated with the ratio of the two isomers.

We then attempted the Bingel functionalization of *trans*-1-bis-Pn-C_{60} (**4**). The first requisite was to perform its encapsulation, but even using the more adaptable Cu^{II}-based nanocapsule **1b**·$(BArF)_8$, encapsulation was reached to a minimum extent, and only minor amounts of encapsulated **4** were detected by HRMS. This was somehow expected from the computational modeling and MD analyses that described that the vertically aligned Pn moieties perpendicular to the porphyrins stand out from the nanocage (Figures 4D and S81B), thus sterically hindering the squeezing of the *trans*-1 compound to the nanocapsule. Therefore, we turned our focus into the Bingel cyclopropanation of encapsulated mono-Pn-C_{60} (**3**), which was successfully encapsulated in **1a**·$(BArF)_8$ (Figures S12–S14). The heterofunctionalization was monitored by HRMS (Figure 8B), clearly showing that a tris-adduct, i.e., mono-Pn-bis-diethylmalonate-C_{60}, was accumulated. The equatorial hetero-tetrakis-adduct was formed in only tiny amounts, despite pushing the experimental conditions (heating and larger reaction times). Upon release of the product from the nanocapsule by solvent washing, full NMR, UV-vis, and MALDI-MS unambiguously led to the conclusion that *e*-mono-Pn-*trans*-1-bis-diethylmalonate-C_{60} (**7**) was obtained as a unique regioisomer in a 63% yield (Figures 8, S40–S50, and S68). The singlet at 5.86 ppm of the ^1H NMR spectrum of **7** clearly indicates a highly symmetric *trans*-1 disposition of the cyclopropanated addends.

Once the supramolecular mask strategy for selective regiofunctionalization combining DA and Bingel addends was demonstrated, we sought to prepare hetero-hexakis-adducts[27,28] by taking advantage of the directing ability of the DA addends of *e,e*-bis-An-C_{60} (**2**) and *trans*-1-bis-Pn-C_{60} (**4**) bis-adducts. First, *e,e*-bis-An-C_{60} (**2**) in solution was subjected to exhaustive Bingel cyclopropanation (40 equiv bromomalonate, 40 equiv DBU, CH_2Cl_2, room temperature, 48 h) to minimize the formation of hetero-tetrakis- and pentakis-adducts. In this manner, hetero-hexakis
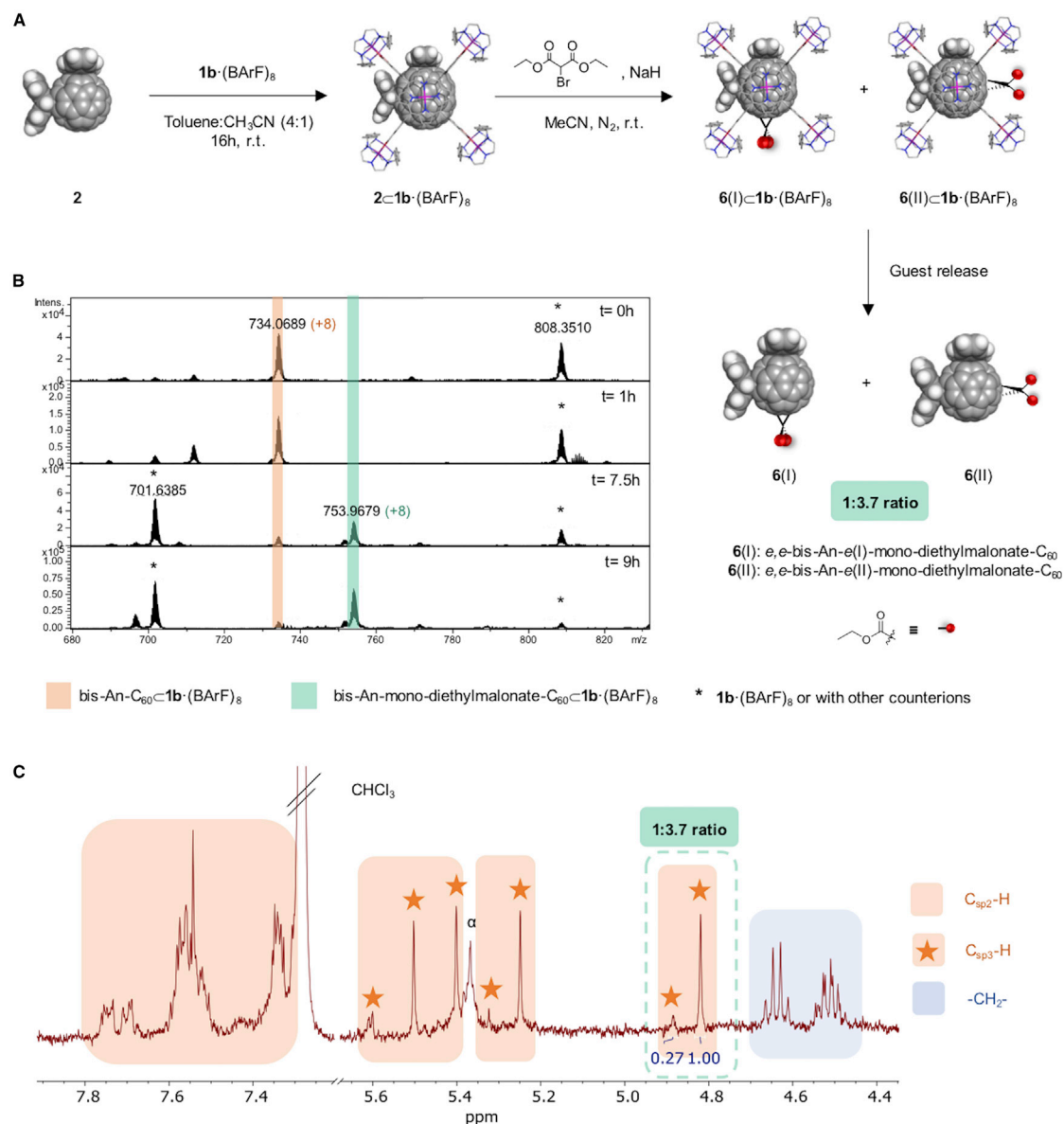
Figure 7. Synthesis and characterization of *e,e*-bis-An-*e*-mono-diethylmalonate-C$_{60}$ (mixture of isomers 6(I) and 6(II))

(A) Schematic representation of the synthesis of **6**.

(B) HRMS monitoring of the synthesis of **6**⊂**1b**·(BArF)$_8$.

(C) ^{1}H NMR of isomers **6**(I) and **6**(II) in a 1:3.7 ratio. In orange, signals corresponding to protons of anthracene addends (highlighting with a star the cycloadded C$_{sp3}$ protons); in blue, signals corresponding to protons of Bingel. See also Figures S29–S39.

adducts (two Ans and four cyclopropanated addends) were mainly formed as assessed by HPLC, MALDI-MS, and 2D NMR (12.5% yield) (Figure 9A, S51–S58, and S68). Specifically, the 2:1:1 pattern corresponding to the cycloadded C$_{sp3}$ proton signals of the An addends remained intact. Therefore, the symmetry featured by the *e,e*-bis-An units suggests that the octahedral-arranged *Th*-hexakis-isomer, i.e., *e,e*-bis-An-based hetero-hexakis-C$_{60}$ (**8**), is mainly obtained.

Finally, emulating Kräutler's orthogonal transposition,[9] *trans*-1-bis-Pn-C$_{60}$ (**4**) was also subjected to exhaustive Bingel cyclopropanation. The expected *Th*-hetero-hexakis-adduct (Figure 9B), i.e., *trans*-1-bis-Pn-*e,e,e,e*-tetrakis-diethylmalonate-C$_{60}$ (**9**), was
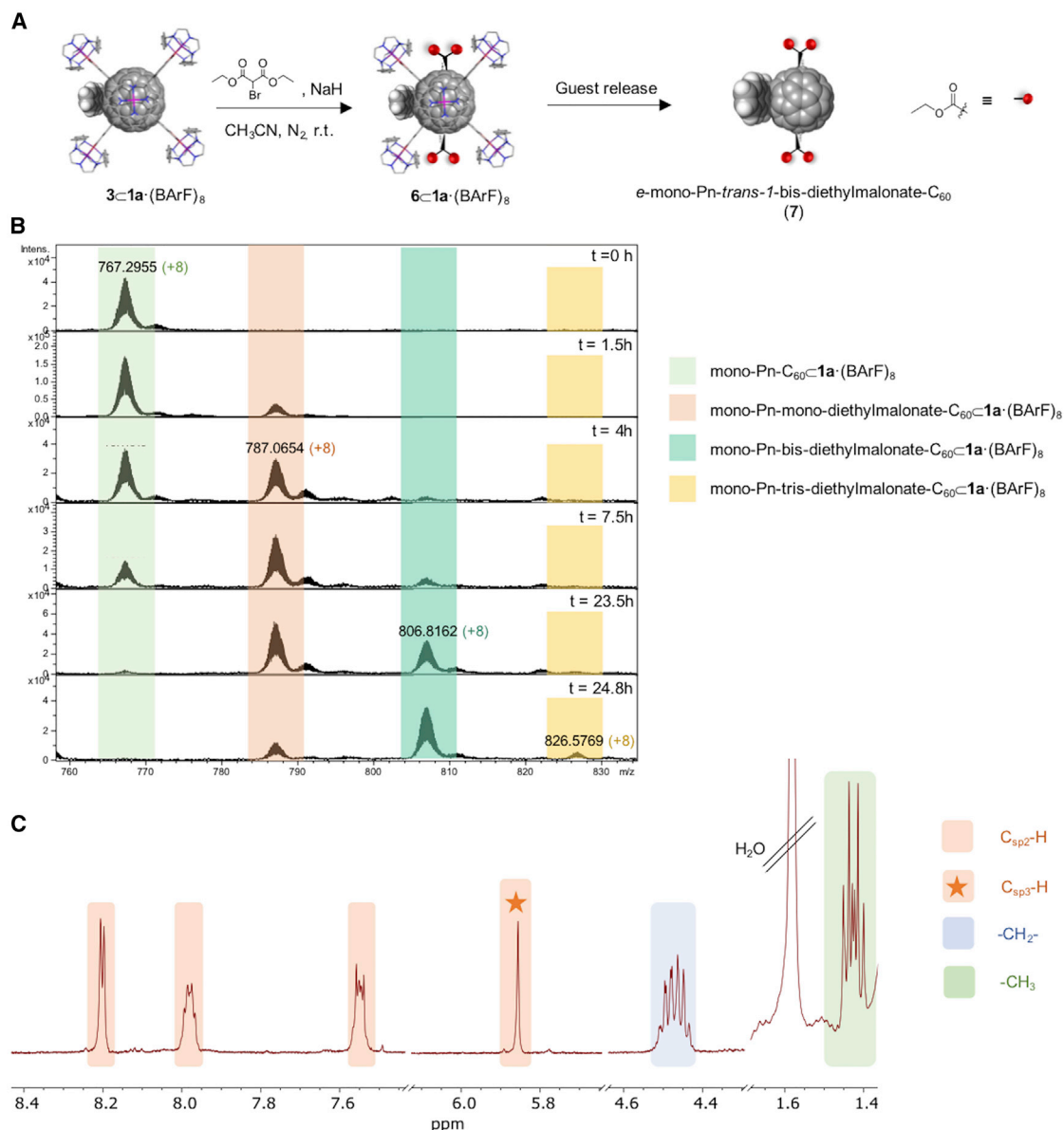
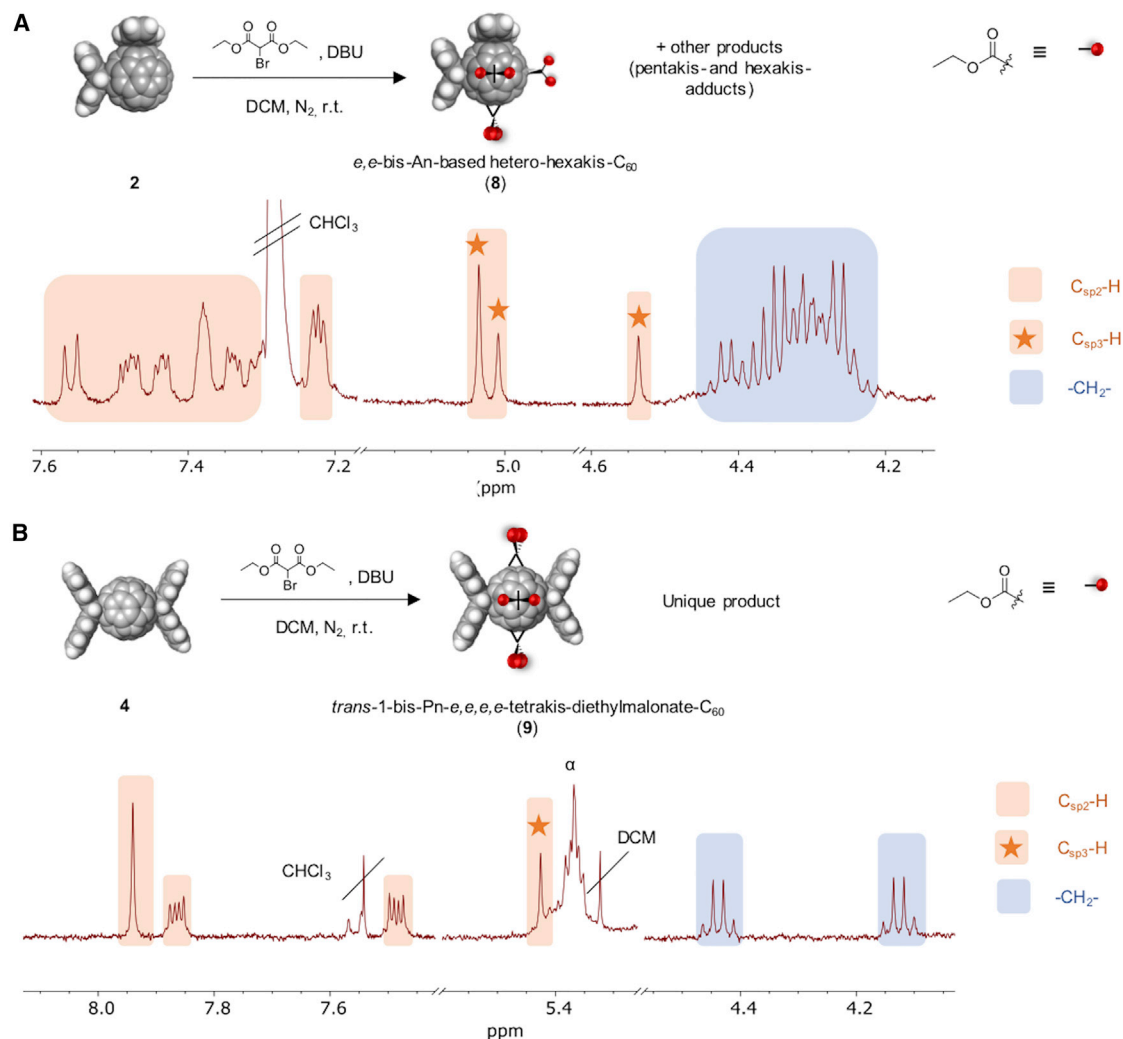**Figure 8. Synthesis and characterization of *e*-mono-Pn-*trans*-1-bis-diethylmalonate-C$_{60}$ (7)**

(A) Schematic representation of the synthesis of **7**.

(B) HRMS monitoring of the synthesis of **7**⊂**1a**·(BArF)$_8$.

(C) ^{1}H NMR of **7**. In orange, signals corresponding to protons of pentacene addends (highlighting with a star the cycloadded C$_{sp3}$ protons); in blue and green, protons of Bingel addends. See also Figures S40–S50.

formed as the unique product (MALDI-MS and 2D NMR, see Figures S59–S68) featuring all four cyclopropanated addends in the equatorial belt of the fullerene, although the yield was low due to insolubility issues of the starting material (**4**). Notably, diffusion coefficients extracted from diffusion-ordered NMR spectroscopy (DOSY-NMR) of bis-, tris-, and hexakis-homo- and heteroadducts (compounds **2–9**) were in strong agreement with the increasing bulkiness of the molecules (Figure S68).

In summary, we have demonstrated that the supramolecular mask strategy for the regiofunctionalization of C$_{60}$ can be extended to DA cycloadditions using tetragonal

Figure 9. Synthesis and characterization of hetero-hexakis-adducts 8 and 9

(A) Schematic representation of the synthesis of the e,e-bis-An-based T_h-hetero-hexakis-C_{60} (**8**) and the corresponding ^{1}H NMR. In orange, signals corresponding to protons of anthracene addends (highlighting with a star the cycloadded C_{sp3} protons); in blue, protons of the Bingel addend. See also Figures S51–S58.

(B) Schematic representation of the synthesis of $trans$-1-bis-Pn-e,e,e,e-tetrakis-diethylmalonate-C_{60} (**9**) and the corresponding ^{1}H NMR. In orange, signals corresponding to protons of pentacene addends (highlighting with a star the cycloadded C_{sp3} protons); in blue, protons of the Bingel addend. See also Figures S59–S67.

prismatic nanocapsules. Moreover, the ability to orthogonally switch the regioselectivity of bis-acene-adducts from 90° (e,e-bis-An-C_{60} [**2**]) to 180° ($trans$-1-bis-Pn-C_{60} [**4**]) by simply enlarging the acene molecule is unprecedented. Computational modeling showed that the differences in the regioselectivity are induced by the different host-guest interactions established between the first formed An- and Pn-based mono-adducts with the nanocapsule. The complementary experimental characterization and computational modeling have proved to be an ideal combination to tackle the comprehension, but also for designing the orthogonal regioselectivity exhibited by these systems. In this manner, the hetero-DA fully equatorial bis-adduct e,e-bis-An-Pn-C_{60} (**5**) is formed.

Furthermore, otherwise inaccessible DA and Bingel poly-heteroadducts were also obtained as equatorial tris-adducts (e,e-bis-An-e-mono-diethylmalonate-C_{60} [**6**] and

e-mono-Pn-*trans*-1-bis-diethylmalonate-C_{60} [**7**]) upon submitting encapsulated bis-adduct **2** and mono-adduct **3** to Bingel cyclopropanation conditions. In this manner, we show here the validity and versatility of the supramolecular mask strategy combining different addends type and different experimental conditions. Finally, bare *e,e*-bis-An-C_{60} (**2**) and *trans*-1-bis-Pn-C_{60} (**4**) were used to build molecular complexity upon them, obtaining the corresponding *Th*-hexakis isomers, i.e., *e,e*-bis-An-based *Th*-hetero-hexakis-C_{60} (**8**) and *trans*-1-bis-Pn-*e,e,e,e*-tetrakis-diethylmalonate-C_{60} (**9**).

This work further exemplifies that tailored supramolecular masks are a promising synthetic strategy for the development of general regioselective crafting of spheroidal fullerenes, which are not accessible by other methodology and will find ample applications in many fields, such as photovoltaics, material science, or biomedicine.

EXPERIMENTAL PROCEDURES

Resource availability

Lead contact
Further information and requests for resources and reagents should be directed to and will be fulfilled by the lead contact, Xavi Ribas (xavi.ribas@udg.edu).

Materials availability
All materials generated in this study are being made available upon reasonable request to the lead contact.

Data and code availability
All the necessary data supporting the main findings of the paper are available within the main paper and its supplemental experimental procedures and from the lead contact upon reasonable request.

Synthesis of *e,e*-bis-An-C_{60} (2)
An (30 equiv, 12.6 mg, 70.5 µmol) was added to a solution of $C_{60} \subset$ **1a**·(BArF)$_8$ (32 mg, 2.35 µmol) in 2.5 mL dry CH_3CN and the reaction was stirred for 48 h at 50°C under N_2. Then, the crude was cooled down in the freezer and filtered and the solvent was removed using a N_2 flow (without heat). The guests were released from the nanocapsules by suspending the remaining solid with chloroform and sonicating the suspension for 15 min. Finally, the suspension was filtered and the products (mono-adduct-C_{60} and *e,e*-bis-adduct-C_{60}) were purified through preparative TLC using CS_2:hexane (3:1) as eluent. It is important to avoid heat during all the workup to avoid retro-DA and also the promotion of tris-adducts. Yield (calculated by HPLC using C_{60} as internal standard) was 38%.

Synthesis of mono-Pn-C_{60} (3)
The synthesis of **3** was carried out with procedures already reported in the literature.[25,29] Fullerene C_{60} (40 mg, 55.5 µmol) and Pn (1.1 equiv, 17 mg, 61 µmol) were refluxed under a N_2 atmosphere in toluene for 48 h. Then, the crude reaction was concentrated under vacuum at low temperatures (maximum of 35°C) and was purified through a chromatographic column using carbon disulfide and hexane (1:1) as eluent. Yield was 32%.

Synthesis of *trans*-1-bis-Pn-C_{60} (4)
Pn (3.4 mg, 12.30 µmol) was added to a solution of $C_{60} \subset$ **1a**·(BArF)$_8$ (74.3 mg, 5.86 µmol) in 7.25 mL dry CH_3CN/CH_2Cl_2 (4:1) and the reaction was stirred for 16 h at 65°C under a N_2 atmosphere. Then, the crude was cooled down in the freezer and filtered and trifluoromethanesulfonic acid (20 equiv) was added and the mixture

was stirred for 45 min to disassemble the **1a**·(BArF)$_8$ cage and release the products. The solvent was removed using a N$_2$ flow (without heat) and the guests were recovered by suspending the remaining solid with carbon disulfide and sonicating it for 15 min. The major product (**4**) was purified through two preparative TLCs. The first used a mixture of carbon disulfide and hexane (3:1) and the second used a mixture of hexane and dichloromethane (1:1). To avoid the promotion of tris-adducts, it is important to avoid the use of heat. Yield of **4** was 30% (calculated by HPLC using C$_{60}$ as internal standard; the HPLC spectrum of the crude mixture [Figure S15] indicates that the main peak of the bis-adduct region corresponds to **4**, although its insolubility allows for the isolation of only a 30% yield).

Synthesis of *e,e*-bis-An-Pn-C$_{60}$ (5)
Pn (1.27 mg, 4.56 μmol) was added to a solution of mono-An-C$_{60}$⊂**1a**·(BArF)$_8$ (50.75 mg, 4.15 μmol) in 4.15 mL dry CH$_3$CN/CH$_2$Cl$_2$ (4:1) and the reaction was stirred for 16 h at 45°C under a N$_2$ atmosphere. Then, the crude was cooled down in the freezer and filtered and trifluoromethanesulfonic acid (20 equiv) was added and the mixture was stirred for 45 min to disassemble the **1a**·(BArF)$_8$ cage and release the products. The solvent was removed using a N$_2$ flow (without heat) and the guests were recovered by suspending the remaining solid with carbon disulfide and sonicating it for 15 min. The major product (**5**) was purified through a preparative TLC using a mixture of carbon disulfide and hexane (3:1). To avoid the promotion of tris-adducts, it is important to avoid the use of heat. Isolated yield was 16%.

Synthesis of *e,e*-bis-An-*e*-mono-diethylmalonate-C$_{60}$ (6)
Two stock solutions of diethyl bromomalonate and sodium hydride in dry acetonitrile were prepared. Then, 5.25 equiv of diethyl bromomalonate and NaH from these solutions were added to a solution of mono-An-C$_{60}$⊂**1b**·(BArF)$_8$ (19 mg, 1.49 μmol) in 1.6 mL of dry acetonitrile at room temperature. After the reaction was monitored by HRMS for 9 h, the solvent was removed under a N$_2$ flow. The guests were released from the nanocapsule by suspending the remaining solid with chloroform (guests in solution and cage in the solid state) and sonicating the suspension for 15 min. Finally, the suspension was filtered and the products (both isomers of hetero-tris-C$_{60}$) were purified through preparative TLC using toluene as eluent. The empty cage was recovered passing acetonitrile through the filter. Yield of **6** was 41% (**6**(I) + **6**(II) mixture and calculated by HPLC using C$_{60}$ as internal standard).

Synthesis of mono-Pn-*e,e*-bis-diethylmalonate-C$_{60}$ (7)
Two stock solutions of diethyl bromomalonate and sodium hydride in dry acetonitrile were prepared. Then, 2.2 and 2.5 equiv of diethyl bromomalonate and NaH, respectively, from these solutions were added to a solution of mono-Pn-C$_{60}$⊂**1a**·(BArF)$_8$ (10.2 mg, 0.78 μmol) in 0.8 mL of dry acetonitrile. After the reaction was monitored by HRMS for 24 h, diethyl ether was added to suspend the host-guest complex. Then, the suspension was filtered through Celite in a pipette. The solid remaining in the filter was washed with chloroform until the filtrate was completely colorless. A preparative TLC using toluene:ethyl acetate (95:5) was performed to eliminate the traces of hetero-bis-adduct and the remaining hetero-tetrakis-adduct. The empty cage was recovered passing acetonitrile through the filter. Yield of **7** was 63% (calculated by HPLC using C$_{60}$ as internal standard).

Synthesis of hexakis-An-C$_{60}$ (8)
The synthesis of **8** was carried out with procedures already reported in the literature.[9] Two stock solutions of diethyl bromomalonate and 1,8-diazabicyclo(5.4.0)

undec-7-ene (DBU) in dry dichloromethane were prepared. Then, 20 equiv of these solutions were added to a suspension of **2** (0.95 mg, 0.88 μmol) in dichloromethane under a N_2 atmosphere at room temperature. After 24 h, 20 equiv more of both stock solutions were added. After 24 h more, the solvent was removed with a N_2 flow and the crude reaction was purified through a preparative TLC to remove the excess of diethyl bromomalonate and DBU. Yield of **8** was 12.5% (calculated by ^{1}H NMR using mesitylene-D_{12} as internal standard).

Synthesis and characterization of _trans_-1-bis-Pn-_e,e,e,e_-tetrakis-diethylmalonate-C$_{60}$ (9)

The synthesis of **9** was carried out with analog procedures already reported in the literature.[9] Two stock solutions of diethyl bromomalonate and DBU in dry dichloromethane were prepared. Then, 20 equiv of these solutions were added to a suspension of **3** (2 mg, 1.6 μmol) in dichloromethane under a N_2 atmosphere at room temperature. After 24 h, 20 equiv more of both stock solutions were added. After 24 h more, the solvent was removed with a N_2 flow and the crude reaction was purified through a preparative TLC to remove the excess of diethyl bromomalonate and DBU. The precise yield could not be calculated due to the small quantities used and the low solubility of the pure initial reactant.

SUPPLEMENTAL INFORMATION

Supplemental information can be found online at https://doi.org/10.1016/j.xcrp.2022.100992.

AUTHOR CONTRIBUTIONS

M.P. performed the synthesis and characterization of all homo- and heteroadducts involving pentacene addends. T.P. performed the synthesis and characterization of all homo- and heteroadducts involving anthracene addends. C.F. performed the initial tests for the Diels-Alder regioselective functionalization with supramolecular masks. T.P. performed all the NMR characterizations of homo- and heteroadducts synthesized. M.G.-B. performed all the MD and electronic structure calculations and related computational analyses and wrote the manuscript. X.R. directed the work, designed the experiments, and wrote the manuscript.

DECLARATION OF INTERESTS

The authors declare no competing interests.

REFERENCES

1. Hirsch, A., and Brettreich, M. (2005). Fullerenes, Chemistry and Reactions (Wiley-VCH).

2. Djojo, F., Hirsch, A., and Grimme, S. (1999). The Addition Patterns of C60 Trisadducts Involving the Positional Relationships e and trans-n (n = 2–4): isolation, Properties, and Determination of the Absolute Configuration of Tris(malonates) and Tris[bis(oxazolines)]. Eur. J. Org. Chem. 1999, 3027–3039.

3. Djojo, F., Herzog, A., Lamparth, I., Hampel, F., and Hirsch, A. (1996). Regiochemistry of twofold additions to [6, 6] bonds in C60: influence of the addend-independent cage distortion in 1, 2-monoadducts. Chem. Eur. J. 2, 1537–1547.

4. Hirsch, A., Lamparth, I., and Karfunkel, H.R. (1994). Fullerene chemistry in three dimensions: isolation of seven regioisomeric bisadducts of C60 and Di(ethoxycarbonyl)methylene. Angew. Chem. Int. Ed. Engl. 33, 437–438.

5. Yan, W., Seifermann, S.M., Pierrat, P., and Bräse, S. (2015). Synthesis of highly functionalized C60 fullerene derivatives and their applications in material and life sciences. Org. Biomol. Chem. 13, 25–54.

6. Fuertes-Espinosa, C., Pujals, M., and Ribas, X. (2020). Supramolecular purification and regioselective functionalization of fullerenes and endohedral metallofullerenes. Chem 6, 3219–3262.

7. Isaacs, L., Diederich, F., and Haldimann, R.F. (1997). Multiple Adducts of C60 by Tether-Directed Remote Functionalization and synthesis of soluble derivatives of new carbon allotropes Cn(60+5). Helv. Chim. Acta 80, 317–342.

8. Isaacs, L., Haldimann, R.F., and Diederich, F. (1994). Tether-directed remote functionalization of buckminsterfullerene: regiospecific hexaadduct formation. Angew. Chem. Int. Ed. Engl. 33, 2339–2342.

9. Schwenninger, R., Müller, T., and Kräutler, B. (1997). Concise route to symmetric multiadducts of [60]Fullerene: preparation of an equatorial tetraadduct by orthogonal transposition. J. Am. Chem. Soc. 119, 9317–9318.

10. Kräutler, B., Müller, T., Maynollo, J., Gruber, K., Kratky, C., Ochsenbein, P., Schwarzenbach, D., and Bürgi, H.B. (1996). A topochemically controlled, regiospecific fullerene bisfunctionalization. Angew. Chem. Int. Ed. Engl. 35, 1204–1206.

11. Trinh, T.M.N., Schillinger, F., Guerra, S., Meichsner, E., Nierengarten, I., Hahn, U., Holler, M., and Nierengarten, J. (2021). Regioselective preparation of fullerene bis-adducts from cleavable macrocyclic bis-malonates. Eur. J. Org. Chem. 2021, 3770–3786.

12. Meichsner, E., Schillinger, F., Trinh, T.M.N., Guerra, S., Hahn, U., Nierengarten, I., Holler, M., and Nierengarten, J. (2021). Regioselective synthesis of fullerene tris-adducts for the preparation of clickable fullerene [3:3]-Hexa-adduct scaffolds. Eur. J. Org. Chem. 2021, 3787–3797.

13. García-Simón, C., Garcia-Borràs, M., Gómez, L., Parella, T., Osuna, S., Juanhuix, J., Imaz, I., Maspoch, D., Costas, M., and Ribas, X. (2014). Sponge-like molecular cage for purification of fullerenes. Nat. Commun. 5, 5557.

14. Fuertes-Espinosa, C., García-Simón, C., Pujals, M., Garcia-Borràs, M., Gómez, L., Parella, T., Juanhuix, J., Imaz, I., Maspoch, D., Costas, M., and Ribas, X. (2020). Supramolecular fullerene sponges as catalytic masks for regioselective functionalization of C60. Chem 6, 169–186.

15. Jiao, Y., Chen, X.-Y., and Stoddart, J.F. (2022). Weak bonding strategies for achieving regio- and site-selective transformations. Chem 8, 414–438. https://doi.org/10.1016/j.chempr.2021.12.012.

16. Ubasart, E., Borodin, O., Fuertes-Espinosa, C., Xu, Y., García-Simón, C., Gómez, L., Juanhuix, J., Gándara, F., Imaz, I., Maspoch, D., et al. (2021). A three-shell supramolecular complex enables the symmetry-mismatched chemo- and regioselective bis-functionalization of C60. Nat. Chem. 13, 420–427.

17. Leonhardt, V., Fimmel, S., Krause, A.-M., and Beuerle, F. (2020). A covalent organic cage compound acting as a supramolecular shadow mask for the regioselective functionalization of C60. Chem. Sci. 11, 8409–8415.

18. Fuertes-Espinosa, C., García-Simón, C., Castro, E., Costas, M., Echegoyen, L., and Ribas, X. (2017). A copper-based supramolecular nanocapsule that enables straightforward purification of Sc3N-based endohedral metallofullerene soots. Chemistry 23, 3553–3557.

19. Fuertes-Espinosa, C., Gómez-Torres, A., Morales-Martínez, R., Rodríguez-Fortea, A., García-Simón, C., Gándara, F., Imaz, I., Juanhuix, J., Maspoch, D., Poblet, J.M., et al. (2018). Purification of uranium-based endohe-dral metallofullerenes (EMFs) by selective su-pramolecular encapsulation and release. Angew. Chem. Int. Ed. Engl. 57, 11294–11299.

20. García-Simón, C., Colomban, C., Çetin, Y.A., Gimeno, A., Pujals, M., Ubasart, E., Fuertes-Espinosa, C., Asad, K., Chronakis, N., Costas, M., et al. (2020). Complete dynamic reconstruction of C60, C70, and (C59N)2 encapsulation into an adaptable supramolecular nanocapsule. J. Am. Chem. Soc. 142, 16051–16063.

21. Duarte-Ruiz, A., Müller, T., Wurst, K., and Kräutler, B. (2001). The bis-adducts of the [5, 6]-fullerene C60 and anthracene. Tetrahedron 57, 3709–3714.

22. Tsuda, M., Ishida, T., Nogami, T., Kurono, S., and Ohashi, M. (1993). Isolation and characterization of Diels–Alder adducts of C60 with anthracene and cyclopentadiene. J. Chem. Soc. Chem. Commun. 1296–1298. https://doi.org/10.1039/C39930001296.

23. Hoffmann, R., and Woodward, R.B. (1965). Selection rules for concerted cycloaddition reactions. J. Am. Chem. Soc. 87, 2046–2048.

24. Seeman, J.I. (2015). Woodward–Hoffmann's stereochemistry of electrocyclic reactions: from day 1 to the JACS receipt date (may 5, 1964 to November 30, 1964). J. Org. Chem. 80, 11632–11671.

25. Mack, J., and Miller, G.P. (1997). Synthesis and characterization of a C60-pentacene monoadduct. Fuller. Sci. Technol. 5, 607–614.

26. Murata, Y., Kato, N., Fujiwara, K., and Komatsu, K. (1999). Solid-state [4 + 2] cycloaddition of fullerene C60 with condensed aromatics using a high-speed vibration milling technique. J. Org. Chem. 64, 3483–3488.

27. Hirsch, A., and Vostrowsky, O. (2001). C60 hexakisadducts with an octahedral addition pattern − A new structure motif in organic chemistry. Eur. J. Org. Chem. 2001, 829–848.

28. Hirsch, A., Lamparth, I., Groesser, T., and Karfunkel, H.R. (1994). Regiochemistry of multiple additions to the fullerene core: synthesis of a Th-symmetric hexakis adduct of C60 with bis(ethoxycarbonyl)methylene. J. Am. Chem. Soc. 116, 9385–9386.

29. Cataldo, F., García-Hernández, D.A., and Manchado, A. (2015). On the C60 fullerene adduct with pentacene: synthesis and stability. Fuller. Nanotub. Carbon Nanostruct. 23, 818–823.